Applied Catalysis B: Environmental 147 (2014) 111–123

Contents lists available at ScienceDirect

Applied Catalysis B: Environmental

journal homepage: www.elsevier.com/locate/apcatb

Chemical deactivation of Fe-BEA as NH_3-SCR catalyst—Effect of phosphorous

Soran Shwan [a,*], Jonas Jansson [b], Louise Olsson [a], Magnus Skoglundh [a]

[a] Competence Centre for Catalysis, Chalmers University of Technology, SE-412 96 Gothenburg, Sweden
[b] Volvo Group Trucks Technology, SE-40508 Gothenburg, Sweden

ARTICLE INFO

Article history:
Received 7 June 2013
Received in revised form 13 August 2013
Accepted 26 August 2013
Available online 1 September 2013

Keywords:
Phosphorous
Chemical deactivation
Poisoning
NH_3-SCR
Fe-BEA
XPS

ABSTRACT

Fe-BEA as catalyst for selective catalytic reduction (SCR) of NO_X with NH_3 was experimentally studied with focus on chemical deactivation caused by phosphorous exposure. Cordierite supported Fe-BEA samples were exposed to 10 or 50 ppm H_3PO_4 for 14, 24 and 48 h in a continuous gas flow reactor at 350 °C. The catalytic activity of the samples was studied by NH_3- and NO-oxidation, NH_3 inhibition and NH_3-SCR experiments. The phosphorous exposed samples were further characterized by NH_3- and NO-TPD, XPS and XRD. The results from the activity studies show that the degree of deactivation due to phosphorous exposure is strongly dependent on the exposure time, while the rate of deactivation is the same for exposure with 10 and 50 ppm H_3PO_4. The XPS results show that primarily phosphorous pentoxides (P_2O_5) are formed after short time of phosphorous exposure while longer time of exposure results in formation of metaphosphates (PO_3^-). The relative amount of metaphosphates after 48 h of H_3PO_4 exposure was about 45% compared to phosphorous pentoxides. The storage capacity of NO was shown to decrease with increasing relative amount of metaphosphates.

The activity studies show that longer time of phosphorous exposure results in significantly decreased activity indicating that the active iron species are very sensitive to phosphorous forming metaphosphates. We suggest that metaphosphates replace the hydroxyl groups on the active iron species in Fe-BEA as the main mechanism for the decreased activity for NH_3-SCR in connection with phosphorous exposure. Furthermore, the NH_3 inhibition experiments show that the increased amount of strongly bound ammonia due to phosphorous exposure does not contribute to buffer the active iron sites with ammonia during transient SCR conditions.

1. Introduction

Selective catalytic reduction with ammonia (NH_3-SCR) using vanadia-based catalysts is a well-established and effective method to eliminate nitrogen oxides (NO_X) in oxygen excess for stationary and mobile applications [1]. However, problems including catalyst ageing and also the toxicity of vanadia, which may form volatile compounds at high temperatures, have promoted the development of alternative catalysts, especially for mobile applications [1]. Copper [2–7] and iron [1,3,8–11] exchanged zeolites, have in this connection proven to be very active and promising alternatives to vanadia in SCR catalysts [1,12,13]. Copper-based zeolites are generally more active for low-temperature SCR compared to zeolites based on iron, which in turn are more active for SCR at higher temperatures. Furthermore, higher SCR performance has been shown for iron-exchanged zeolites under transient conditions (e.g. ammonia pulsing) by Kamasamudram et al. when copper- and iron-based zeolites were compared [14]. Recently, promising results have been shown for simultaneously exchanged Fe/Cu zeolites combining the advantages of both metals in the same catalyst [15].

Several challenges arise when using these materials in aftertreatment systems for diesel and lean burn vehicles. Two of the more important issues are the tolerance against chemical poisoning and the hydrothermal stability of the ion-exchanged zeolites [1]. Chemical poisoning is strong chemisorption of impurities on the active sites of the catalyst [16], where high tolerance against catalyst poisons such as calcium (Ca), magnesium (Mg), phosphorous (P), sulphur (S) and zinc (Zn), which originate from fuel and lubricating oils, is desired [17]. Another problem related to poisoning is blocking of pores caused by hydrocarbons [18–20], especially during cold-start conditions. However, the resistance of metal-exchanged zeolites towards hydrocarbon poisoning can be enhanced by addition of a protecting layer on the zeolite [18].

Phosphorous, originating mainly from lubricating oils and more recently from the fuel (biofuels) as well, has been shown to damage the aftertreatment systems used for emission control. Due to

* Corresponding author at: Competence Centre for Catalysis and Department of Applied Surface Chemistry, Chalmers University of Technology, SE-41296 Göteborg, Sweden. Tel.: +46 0 31 772 2943.
E-mail address: soran@chalmers.se (S. Shwan).

0926-3373/$ – see front matter © 2013 Elsevier B.V. All rights reserved.
http://dx.doi.org/10.1016/j.apcatb.2013.08.042

the relatively high phosphorous content in many types of biofuels, the American Society for Testing and Materials (ASTM) and European Committee for Standardization (CEN) have set the specification value of 10 ppm as the maximum allowed phosphorous level in biodiesel [21]. Vanadia-based NH_3-SCR catalysts have been thoroughly investigated and most studies of chemical poisoning show a clear correlation between decreased activity for NO_X reduction and exposure of phosphorous and other inorganic poisons [21–28].

Blanco et al. [29] impregnated vanadia-based NH_3-SCR catalysts with H_3PO_4 and showed that even with 15 wt.% phosphorous in the sample, the NO_X conversion was almost unaffected compared to a fresh sample. Similar results were shown by Kröcher and Elsener [22] where a relatively low decrease in NO_X reduction was observed for $V_2O_5/WO_3–TiO_2$ catalysts when doped with phosphoric acid compared to other inorganic poisons. Furthermore, Beck et al. [30] showed that vanadia-based catalysts exposed to flue gases from combustion of phosphorous rich fuels in a full-scale plant contained up to 5 wt.% P_2O_5 on the surface and a significant decrease in NO_X reduction compared to fresh catalysts. The authors suggested that the deactivation by phosphorous occurs due to formation of phosphate glasses (P_2O_5). However, the catalyst was exposed to flue gases from a full-scale plant and it was not possible to clearly point out the main deactivation mechanism due to the presence of other catalyst poisons. Furthermore, Castellino et al. [24] exposed a vanadia-based NH_3-SCR catalyst to phosphorous under more controlled and realistic conditions by adding H_3PO_4 of different concentrations into the feed gas and observed strong deactivation of the catalyst. It was concluded that exposure by phosphoric acid in the flue gas results in much severer degradation when compared to impregnation of the catalyst with phosphoric acid most likely due to both physical and chemical deactivation in the former case.

The open literature contains very few studies of chemical deactivation of metal-exchanged zeolites used as NH_3-SCR catalysts with focus on phosphorous [23,25]. In a recent study by Silver et al. [23], an Fe-zeolite catalyst was exposed to phosphorous enriched fuel (10 g/l) and it was concluded that phosphorous blocks the adsorption of NH_3, resulting in 20% decreased NO_X conversion. It was suggested that the lower NO_X reduction is a result of decreased NH_3 adsorption. Most studies of chemical deactivation attribute the decreased NO_X conversion mainly due to decreased NH_3 storage capacity. Multiple studies of Fe-zeolites [31–35] and as well as of vanadia-based [36,37] catalysts have shown that high storage capacity of ammonia is not required to acquire high NO_X conversion. However, Kern et al. [25] argued that the decreased activity for NO_X reduction of Fe-zeolites poisoned with phosphorous partly could be attributed to decreased NH_3 storage capacity and one should not rule out the interaction of phosphates with Fe-species in the catalyst.

The objective of the present study is to investigate the chemical deactivation of Fe-BEA as NH_3-SCR catalyst with phosphorous under controlled flow-reactor experiments. The samples exposed to phosphorous are studied by NH_3- and NO-oxidation, NH_3-SCR and NH_3 inhibiting experiments. The samples are further characterized by temperature programmed desorption of NH_3 and NO, X-ray photoelectron spectroscopy and X-ray diffraction. Prior to exposure to phosphorous the samples are also studied with UV–vis spectroscopy. The focus is paid on the fundamental chemical deactivation mechanism of the active iron species and therefore the amount of phosphorous exposed to the samples is relatively low to avoid extensive formation of phosphate glasses. The mechanisms for hydrothermal deactivation of Fe-BEA with focus on the active iron sites [31–33,38,39] have recently been studied by our group and the present study will continue on the discussion related to the active iron sites however with focus on the chemical deactivation.

2. Experimental methods

2.1. Sample preparation

For this study an 1 wt.% Fe-BEA catalyst was prepared using incipient wetness impregnation. First 9.9 g H-BEA powder (SAR = 38, Zeolyst International) was dried at 120 °C for 2 h. Then 0.72 g $Fe(NO_3)_3{\cdot}9H_2O$ (Fisher Scientific) was dissolved in 9.9 ml distilled water and mixed carefully with the H-BEA powder. The solution was thereafter dried at 120 °C for 24 h before crushed into a fine powder and calcined in air at 450 °C for 3 h. Seven cordierite monolith substrates (Corning; 400 cpsi; 21 mm in diameter and 20 mm in length) were prepared and calcined in air at 500 °C for 2 h. The monolith substrates were initially washcoated with a thin layer of alumina, using 5 wt.% boehmite (Disperal D Sasol) in a liquid phase of 50 wt.% distilled water and 50 wt.% ethanol to facilitate the adhesion of the catalyst. The samples were then calcined at 500 °C for 2 h. The monolith samples were finally coated with the catalyst by immersing the substrate in a slurry of 20 wt.% solid and 80 wt.% liquid phase (50 wt.% distilled water and 50 wt.% ethanol) where the solid fraction contained 90 wt.% Fe-BEA and 10 wt.% boehmite, and dried in air at 90 °C for 2 min. This procedure was repeated several times until the monolith substrates were coated with the desired amount of washcoat before final calcination at 500 °C for 2 h. Table 1 shows the final amount of washcoat for the prepared samples.

2.2. Phosphorous exposure

The fresh samples were exposed to phosphoric acid (H_3PO_4) in an ageing reactor. The ageing reactor is vertically placed and consists of a preheater and a reactor chamber where the samples are placed. Two thermocouples are placed in the front and at the end of the preheater. The reactor has six thermocouples which are placed above each sample. The gas preheater contains a thermocouple for gas temperature regulation. The reactor has six additional small sample holders were the samples are placed.

The gas flow through the reactor during the phosphorous exposure was 4000 ml/min and consisted of 10 or 50 ppm H_3PO_4 (added to the water), and 10% H_2O, 6% O_2 and N_2 as inert gas with a space velocity (GHSV) of 5250 h^{-1}. Three catalyst samples were exposed to 10 ppm H_3PO_4 at 350 °C for 14, 24 and 48 h, respectively. The remaining three samples were exposed to 50 ppm H_3PO_4 at 350 °C for 14, 24 and 48 h, respectively. One catalyst (denoted fresh) was kept untreated for comparison with the phosphorous exposed samples. Before analysis, all samples (both fresh and phosphorous exposed samples) were degreened in 400 ppm NO, 400 ppm NH_3, 8% O_2 and 5% H_2O at 500 °C for 2 h. The samples exposed to 10 ppm H_3PO_4 are referred to as 14 h (10 ppm), 24 h (10 ppm) and 48 h (10 ppm), and the samples exposed to 50 ppm H_3PO_4 are referred to as 14 h (50 ppm), 24 h (50 ppm) and 48 h (50 ppm) in the figures.

2.3. Flow reactor system

The following experiments were performed to characterize and evaluate the catalytic properties of the samples; Temperature programmed desorption of ammonia and nitric oxide (NH_3- and NO-TPD, respectively), NO- and NH_3-oxidation, selective catalytic reduction of NO_X with ammonia (NH_3-SCR), and NH_3 inhibition experiments.

The NH_3- and NO-TPD experiments, and the experiments for evaluation of the catalytic performance (NH_3- and NO-oxidation, NH_3-SCR and NH_3 inhibition experiments) were performed using a continuous gas flow reactor system which is described in detail in Ref. [2]. Briefly the reactor consists of a horizontal quartz tube, 800 mm long with an inner diameter of 22 mm, equipped with a

Table 1
Phosphorous exposure, washcoat weight, relative amount of PO_3^- and relative amount of Fe^{3+} determined by XPS, and increased NO_X reduction time after ammonia cut-off during NH_3-SCR for all samples.

Sample (H_3PO_4 exposure time and conc.)	Washcoat weight[a] (mg)	$\frac{PO_3^-}{P_2O_5+PO_3^-}$ (%)	$\frac{Fe^{3+}}{Fe^{2+}+Fe^{3+}}$ (%)	Increased SCR period – 200 °C (min)	Increased SCR period – 250 °C (min)
Fresh	725	–	51	13	4
14 h-10 ppm	693	12	50	13	4
24 h-10 ppm	681	27	52	11	3
48 h-10 ppm	682	46	51	16	5
14 h-50 ppm	722	13	50	13	4
24 h-50 ppm	695	39	51	12	3
48 h-50 ppm	698	45	50	14	4

[a] Washcoat weight do not include the mass of the monolith.

heating coil and insulation. The heating unit is regulated by a temperature controller (Eurotherm). The sample is placed in the quartz tube with a thermocouple placed 10 mm in front of the catalyst to control the inlet gas temperature. A second thermocouple is placed inside the centre of the catalyst to measure the sample temperature. The gas mixing system consists of separate mass flow controllers (Bronkhorst) for NO, NH_3, O_2 and Ar. Water is added downstream of the mixed gases in an evaporator which is heated to 150 °C. The amount of water added to the feed is regulated by a mass flow controller (Bronkhorst). Gas phase analysis is performed using a gas phase FTIR spectrometer (MKS 2000 FTIR).

2.4. Catalyst characterization

The H-BEA powder sample and the 1 wt.% Fe-BEA powder catalyst were characterized using UV–vis spectroscopy before washcoated and exposed to phosphoric acid. Spectra were collected using a Cary 5000 UV–vis–NIR spectrophotometer equipped with an external DRA-2500 unit. The integrating sphere permits fast acquisition of high-quality (high-resolution, low-noise) spectra. The spectra were recorded in the 200–1500 nm wavelength range, using the appropriate baseline correction. The UV–vis spectrum of H-BEA was thereafter subtracted from the corresponding Fe-BEA spectrum in order achieve the spectrum for iron. The UV–vis spectra for iron were converted using the Kubelka–Munk function and deconvoluted using a Gaussian function.

After phosphorous exposure the samples were characterized in the flow reactor where NH_3- and NO-TPD experiments, and activity measurements were performed. The samples were further characterized by X-ray photoelectron spectroscopy (XPS) and X-ray diffraction (XRD).

Before each TPD experiment the samples were exposed to 8% O_2 in Ar at 500 °C for 15 min. During the subsequent NH_3- and NO-TPD experiments the sample was exposed to 400 ppm NO or NH_3 and 5% H_2O at 150 °C for 40 min followed by flushing in 5% water in Ar at the same temperature for 30 min. This was followed by a temperature ramp in 5% water in Ar from 150 to 500 °C at a heating rate of 10 °C/min.

X-ray photoelectron spectroscopy was performed to determine the chemical state of phosphorous and iron in the samples. The XPS measurements were performed using a PerkinElmer PHI 5000C ESCA system described in detail in Ref. [40]. The XPS spectra were obtained using monochromatic Al Kα radiation with 45° take-off angle. To perform the experiment, an 1 mm × 5 mm sample was cut out from one of the inner channels of the monolith sample and placed in the pre-treatment chamber whereby the pressure was reduced to about 10^{-9} mbar before transferring the sample to the UHV chamber. The sample pieces were cut from the middle section of the monoliths to achieve a representative part of the phosphorous exposed samples. The P 2p, Fe 2p and O 1s binding energy levels were thoroughly studied. Correction for charging was performed by normalizing the spectra using the C 1s peak at 284.6 eV [41] as reference. Deconvolution of the P 2p and Fe $2p_{3/2}$ peaks from each sample was performed by fitting a Gaussian function to the experimental data. The peak positions were optimized according to the same procedure for all samples to achieve the lowest standard deviation, χ^2, and found to be 134.5 and 135.5 eV for PO_3^- and P_2O_5, respectively, and 710.4 and 712.2 eV for Fe^{2+} and Fe^{3+}, respectively. The fitted peaks are in accordance with other studies summarized in Table 2.

X-ray diffraction was used to identify crystalline phases and to estimate the particle size in the washcoat of the different samples. The instrument used was a Siemens D500 X-ray diffractometer with Bragg-Brentano geometry and a Cu Kα source.

2.5. Activity measurements

Steady-state activity measurements were performed for all samples using a gas composition of 400 ppm NO and/or 400 ppm NH_3, 8% O_2 and 5% water in Ar, in the flow reactor. In all experiments the total gas flow was kept constant at 3500 ml/min which corresponds to a space velocity (GHSV) of 27,600 h^{-1}. Before each experiment the sample was exposed to 8% O_2 in Ar for 15 min at 500 °C.

The activity for NO oxidation was investigated by exposing the sample to 400 ppm NO, 8% O_2 and 5% H_2O whereby the temperature stepwise was increased from 150 to 500 °C (150, 200, 250, 300, 400 and 500 °C). The duration was 40 min for the first step, 30 min for step two and three, and 20 min for the last three temperature steps. The heating rate between each temperature step was 20 °C/min.

The activity for NH_3 oxidation was investigated accordingly by exposing the sample to 400 ppm NH_3, 8% O_2 and 5% H_2O whereby the temperature stepwise was increased from 150 to 500 °C (150,

Table 2
Binding energies for Fe $2p_{3/2}$ and P 2p XPS peak maxima in various studies.

Species	Binding energy [eV]	Reference
Fe(II)O	709	Thomas et al. [54]
	709.5	McIntyre and Zetaruk and Moulder et al. [55,56]
	710.2	Pratt et al. [57]
	710.5	Janas et al. [58]
Fe(III)OOH	711.9	Moulder et al. [55]
$Fe(III)_2O_3$	711.6	McIntyre and Zetaruk [56]
	711	Thomas et al. [54]
	712	Thomas et al. [54]
	712.3	Janas et al. [58]
	712.7	Pratt et al. [57]
	714	Thomas et al. [54]
$P(V)_2O_5$	135.5	Moulder et al. [55]
$P(V)O_3^-$	134.5	Moulder et al. [55]

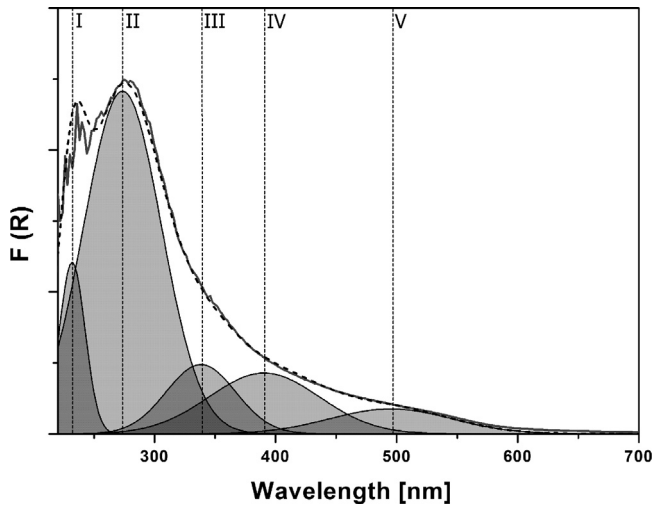

Fig. 1. UV–vis spectrum of iron from the fresh 1 wt.% Fe-BEA powder sample after subtraction of the corresponding spectrum for H-BEA. The deconvoluted peaks (**I** and **II**) represent monomeric iron species (220–290 nm), (**III** and **IV**) dimeric and oligomeric iron species (300–400 nm), and (**V**) larger iron oxide particles (>400 nm).

200, 250, 300, 400 and 500 °C). The duration was 40 min for the first step, 30 min for step two and three, and 20 min for the last three temperature steps. The heating rate between each temperature step was 20 °C/min.

The activity for selective catalytic reduction of NO_X with ammonia (NH_3-SCR) as the reducing agent was studied for all samples. The gas feed consisted of 400 ppm NO, 400 ppm NH_3, 8% O_2 and 5% H_2O. The sample was exposed to the gas mixture at 150 °C for 40 min, 200, 250, and 300 °C for 30 min, and 400 and 500 °C for 20 min. Before stabilization at each temperature step, the temperature did not exceed the set point by more than 4 °C.

For the ammonia inhibition experiments the sample was exposed to the same gas composition as for the NH_3-SCR experiment at 200 and 250 °C for 40 min. The NH_3 feed was then cut off and compensated with inert gas to maintain constant flow. The SCR activity was continuously measured before and after the ammonia cut-off.

3. Results

3.1. Characterization

Diffuse-reflectance UV–vis spectroscopy was used to study the distribution of iron species in the fresh 1 wt.% Fe-BEA catalyst after subtracting a base line for H-BEA. Fig. 1 shows the UV–vis spectrum for iron in the fresh Fe-BEA powder catalyst. The deconvoluted spectrum shows two bands related to isolated Fe^{3+} species in the UV region peaking at 232 and 273 nm, respectively [42,43]. Furthermore, the bands with maxima at 340 and 390 nm are assigned to dimeric iron (Fe^{2+}) species and smaller oligomeric Fe species as Fe_XO_Y, whereas the band at with maximum 496 nm is related to Fe_2O_3 particles located outside the zeolite pores [42,43]. The UV–vis spectrum clearly shows that isolated iron (Fe^{3+}) is the dominating iron species for the fresh 1 wt.% Fe-BEA catalyst. The presence of dimeric iron (Fe^{2+}) is relatively low compared to isolated iron species.

The results from the NH_3-TPD experiments are shown in Figs. 2 and 3. Fig. 2a shows the desorption spectra for the samples exposed to 10 ppm H_3PO_4 and Fig. 2b shows the corresponding spectra for the samples exposed to 50 ppm H_3PO_4. During the storage phase (not shown in Fig. 2) all samples show complete ammonia uptake for about 3.9 min followed by a sloping NH_3

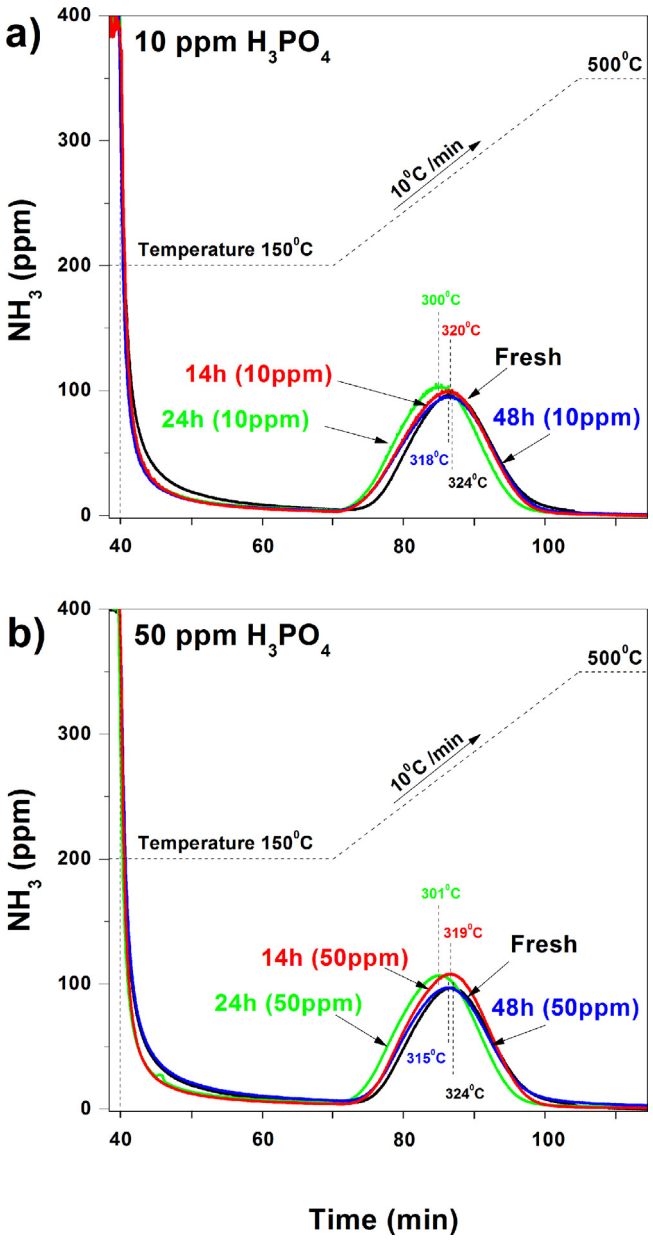

Fig. 2. NH_3 desorption spectra for the studied Fe-BEA samples: (a) catalysts exposed to 10 ppm H_3PO_4 for 14, 24 and 48 h. (b) Catalysts exposed to 50 ppm H_3PO_4 for 14, 24 and 48 h. The samples were exposed to 400 ppm NH_3 and 5% H_2O for 40 min at 150 °C, flushed in 5% H_2O in Ar for 30 min and finally a temperature ramp of 10 °C/min to 500 °C was applied. The total flow rate is 3500 ml/min.

response up to saturation. The ammonia response varies slightly for the samples and thus the NH_3 uptake differs between the samples. Fig. 3a and b summarizes the uptake of ammonia for the samples exposed to 10 and 50 ppm H_3PO_4, respectively, with a total uptake of around 0.5 mmol $NH_3/g_{washcoat}$ for all samples. During the desorption phase of the NH_3-TPD experiment, weakly bound ammonia desorbs during the entire initial period (30 min) at constant temperature for all samples, as shown in Fig. 2. The amount of weakly bound ammonia differs slightly between the fresh and phosphorous exposed samples. Fig. 3 shows that the amount of weakly bound ammonia decreases for the samples exposed for 14 and 24 h. However, for the sample exposed to 50 ppm H_3PO_4 for 48 h the amount of weakly bound ammonia increases to the same level as for the fresh sample. A more pronounced difference between the samples can be seen during the temperature programmed

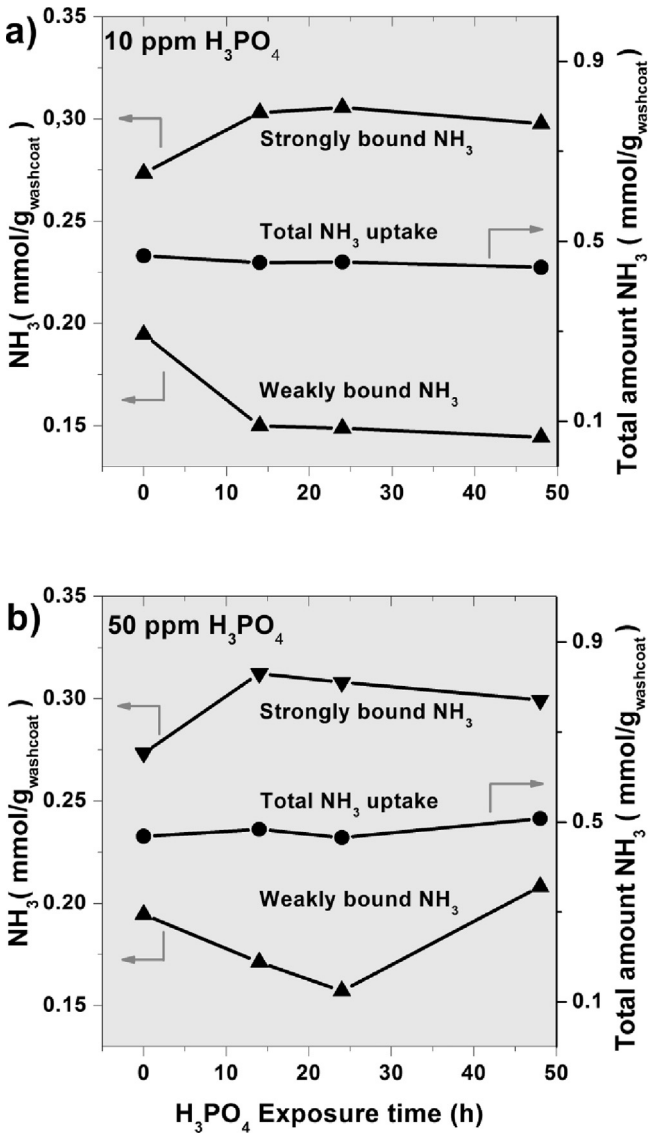

Fig. 3. The amount of weakly and strongly bound ammonia together with the total amount of ammonia desorbed during the NH_3-TPD experiments. The amounts are shown versus the H_3PO_4 exposure time: (a) Fe-BEA samples exposed to 10 ppm H_3PO_4 for 14, 24 and 48 h; (b) Fe-BEA samples exposed to 50 ppm H_3PO_4 for 14, 24 and 48 h.

desorption phase of the experiment. Fig. 2 shows the desorption maximum for the fresh and all phosphorous exposed samples. From the figure it can be observed that the temperature for the desorption maximum decreases for the samples exposed the shortest times (for 14 h and 24 h at both 10 and 50 ppm H_3PO_4) and thereafter increases. A similar trend can be observed in Fig. 3 where the total amount of strongly bound NH_3 is shown. The desorbed amount of strongly bound ammonia increases with increasing phosphorous exposure time (14 and 24 h at 10 and 50 ppm H_3PO_4) and decreases slightly for the samples most severely exposed for phosphorous (48 h).

The XPS spectra for the fresh and phosphorous exposed samples are shown in Fig. 4 and the deconvoluted peaks from the experimental data are shown in Figs. 5 and 6. Fig. 4a shows the P 2p peak with maximum around 135 eV and Fig. 4b shows the Fe $2p_{1/2}$ and Fe $2p_{3/2}$ peaks with maximum around 721 and 709 eV, respectively. In Table 2 the position of the P 2p peak for P_2O_5 and PO_3^-, and the Fe $2p_{3/2}$ peak for FeO, FeOOH and Fe_2O_3 from several studies are summarized. Compared to the fresh sample in Fig. 4a, there is a significant difference for the samples exposed to phosphorous. The intensity of the P 2p peak increases with increasing H_3PO_4 exposure. The positions of the fitted peaks of phosphorous pentoxides, P_2O_5 and metaphosphates, PO_3^-, are marked in Fig. 4a and it can be observed how the P 2p peak slightly shifts towards lower binding energy with increased phosphorous exposure. Furthermore, the P 2p peak of the samples exposed to 50 ppm H_3PO_4 is slightly more intense compared to the samples exposed to 10 ppm phosphoric acid. This is most pronounced for the samples exposed for phosphorous for 48 h. Fig. 5 shows the deconvolution of the XPS spectra of the P 2p peak for all samples. Experimental values are shown as black dots while the sum of the fitted peaks, attributed to P_2O_5 and PO_3^-, is shown by the solid black line. The peak area for P_2O_5 and PO_3^- is marked in dark and light red, respectively. The ratios between the deconvoluted PO_3^- peak and the sum of the P_2O_5 and PO_3^- peaks are summarized in Table 1. There is no significant difference between the samples exposed to 10 or 50 ppm H_3PO_4. However, with increasing exposure time the relative amount of metaphosphates, PO_3^-, compared to phosphorous pentoxides, P_2O_5, increases. The samples exposed to H_3PO_4 for 14 h show a relative amount of PO_3^- of around 12% compared to the samples exposed for 48 h for which the relative amount of PO_3^- is around 45%. Fig. 4b, shows the XPS spectra of the Fe $2p_{3/2}$ peak with the positions of the Fe^{2+} and Fe^{3+} peaks marked. There is no notable or significant difference between the spectra of the fresh and phosphorous exposed samples and the intensity is almost constant. Fig. 6 shows the deconvolution of the XPS spectra of the Fe $2p_{3/2}$ peak for all samples. Experimental values are shown as black dots while the sum of the fitted peaks, attributed to Fe^{2+} and Fe^{3+}, is shown by the solid black line. The area for the fitted Fe^{2+} and Fe^{3+} peak is marked in dark and light orange, respectively. The ratios between the deconvoluted Fe^{3+} peak and the sum of the Fe^{2+} and Fe^{3+} peaks are summarized in Table 1. All samples show a relative amount of Fe^{3+} of about 50%.

X-ray diffraction (not shown) was used to identify crystalline phases in the samples. Compared to the fresh sample the main diffraction peak of zeolite BEA at $2\theta = 22.7^\circ$ [44,45] is almost unchanged for the phosphorous exposed samples. Furthermore, no diffraction peaks at $2\theta = 16.5^\circ$ and 17.2° [46] representing phosphorous pentoxide P_2O_5 can be observed for the samples exposed to phosphoric acid. The results indicate that phosphorous pentoxide, if present, either is non-crystalline or that the particles are too small to be resolved by XRD. Furthermore, no diffraction peaks from Fe_2O_3 at $2\theta = 33.2^\circ$ or 35.5° [20] could be observed, neither for the fresh nor the phosphorous exposed samples which indicates that the present Fe_2O_3 particles observed from the UV–vis study are too small to be identified with XRD or that iron oxide is present as non-crystalline phases.

The results for the NO-TPD experiments are shown in Fig. 7. In contrast to NH_3, the uptake of NO is very low for all samples and there is no period with complete NO uptake. It can further be mentioned that no formation of NO_2 is observed during the experiment. However, during the desorption part of the experiment there is a significant difference between the samples. The amount of NO desorbed decreases with increased exposure time for H_3PO_4. Similar to the previous observation, there is no significant difference between the exposure levels, i.e. the samples exposed to 10 compared to 50 ppm H_3PO_4.

3.2. Oxidation of NH_3 and NO

The results from the NH_3-oxidation experiment, where the samples were exposed to 400 ppm NH_3, 8% O_2 and 5% H_2O, and the temperature stepwise was increased from 150 to 500 °C, are shown in Fig. 8. The outlet concentration of NH_3 from the experiments for the samples exposed to 10 ppm H_3PO_4 are shown in Fig. 8a and

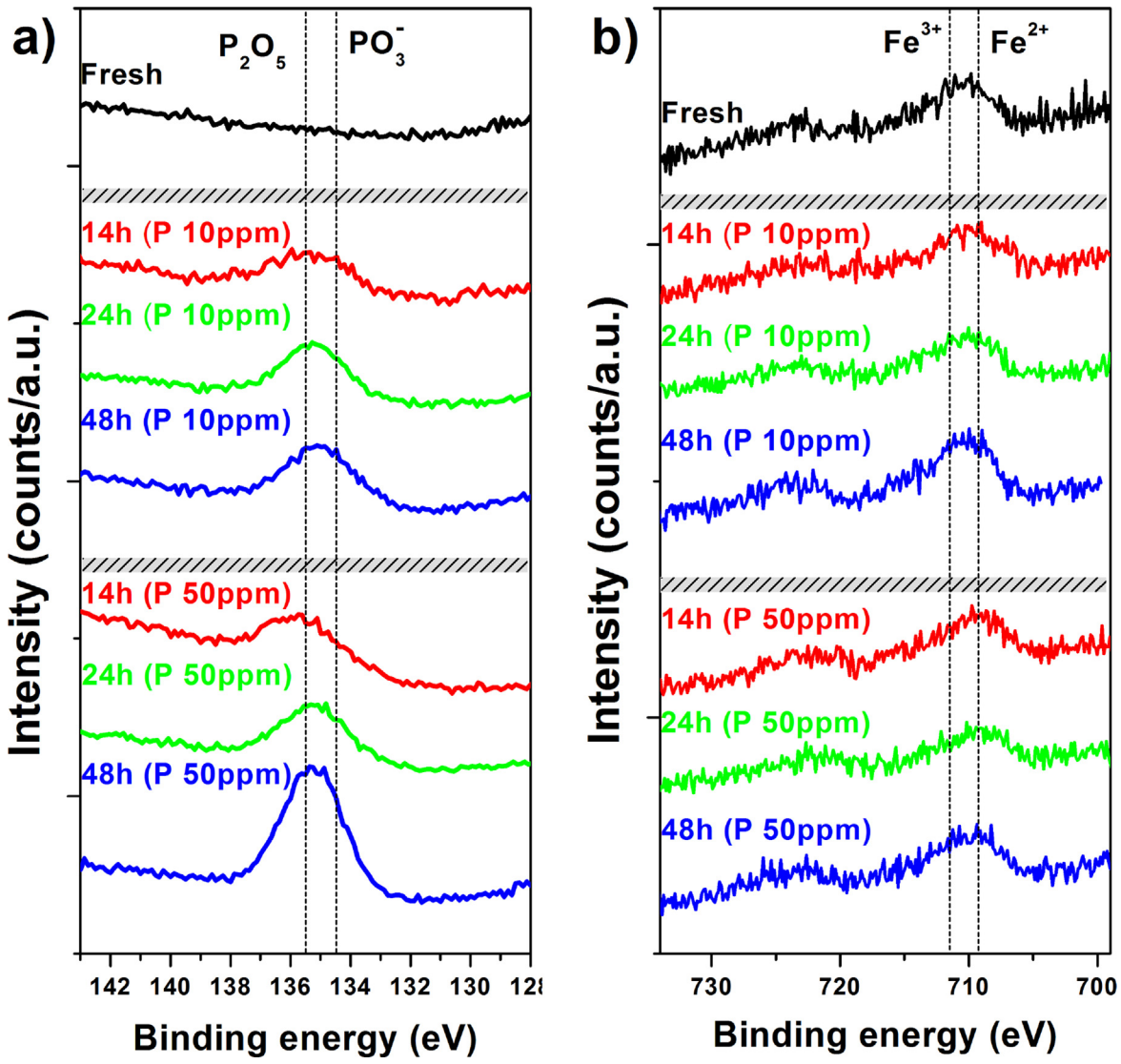

Fig. 4. XPS spectra of the phosphorous exposed Fe-BEA samples: (a) Phosphorous (P 2p) and (b) iron (Fe $2p_{3/2}$ and Fe $2p_{1/2}$) compared to fresh sample. The binding energy for P_2O_5 and PO_3^- is marked with dotted lines at 135.5 and 734.5 eV, respectively. The position of Fe^{2+} and Fe^{3+} is marked with dotted lines at 708.97 and 712.23 eV, respectively.

compared to the fresh sample. At 150 °C ammonia storage can be observed during the initial part of the experiment, similar to the NH_3-TPD experiments and ammonia desorption during the temperature ramp after each temperature step. Further similarities can be observed in the desorption peak between the temperature steps compared to the NH_3-TPD experiments (cf. the NH_3-TPD results in Fig. 3) where the phosphorous exposed samples show desorption of higher amounts of strongly bound ammonia. Furthermore, the ammonia starts to react with oxygen at 400 °C for all samples and at 500 °C the fresh sample shows about 50% ammonia conversion. The effect of phosphorous can be observed for the samples exposed to 10 ppm H_3PO_4 for 14 and 24 h which show about 40% ammonia conversion compared to the sample exposed for 48 h with about 32% conversion. Fig. 8b shows the results for the samples exposed to 50 ppm H_3PO_4 compared to the fresh sample. The results are similar to those for the samples exposed to 10 ppm phosphoric acid where the most severely exposed sample shows an NH_3 conversion around 35%.

The results from the NO-oxidation experiment, where the samples were exposed to 400 ppm NO, 8% O_2 and 5% H_2O, and the temperature stepwise was increased from 150 to 500 °C, are shown in Fig. 9. Fig. 9a and b shows the outlet concentration of NO from the experiments for the samples exposed to 10 and 50 ppm H_3PO_4, respectively. At the lowest temperature, 150 °C, only minor oxidation can be observed for the fresh and least phosphorous exposed samples. However, above 150 °C all samples show activity for NO oxidation. The results are in agreement with previous results in this study (NH_3-oxidation and NH_3-SCR reaction) which show similar activity for both levels of phosphorous exposure. The samples with longest exposure time for 10 or 50 ppm H_3PO_4 (i.e. 48 h) show a more pronounced decrease in NO oxidation activity compared to the fresh sample. At 500 °C, where the activity for NO oxidation is highest, the samples with the longest phosphorous exposure time show about 13% NO conversion compared to 15% for the fresh sample.

3.3. *Selective catalytic reduction of NO_X with NH_3*

The results for the SCR experiments, where the samples were exposed to 400 ppm NO, 400 ppm NH_3, 8% O_2 and 5% H_2O, and the temperature stepwise was increased from 150 to 500 °C, are shown in Figs. 10 and 11. Fig. 10a and b shows the outlet concentration of NO_X and NH_3, respectively, for the samples exposed to 10 ppm H_3PO_4 compared to the fresh sample. At 150 °C the SCR

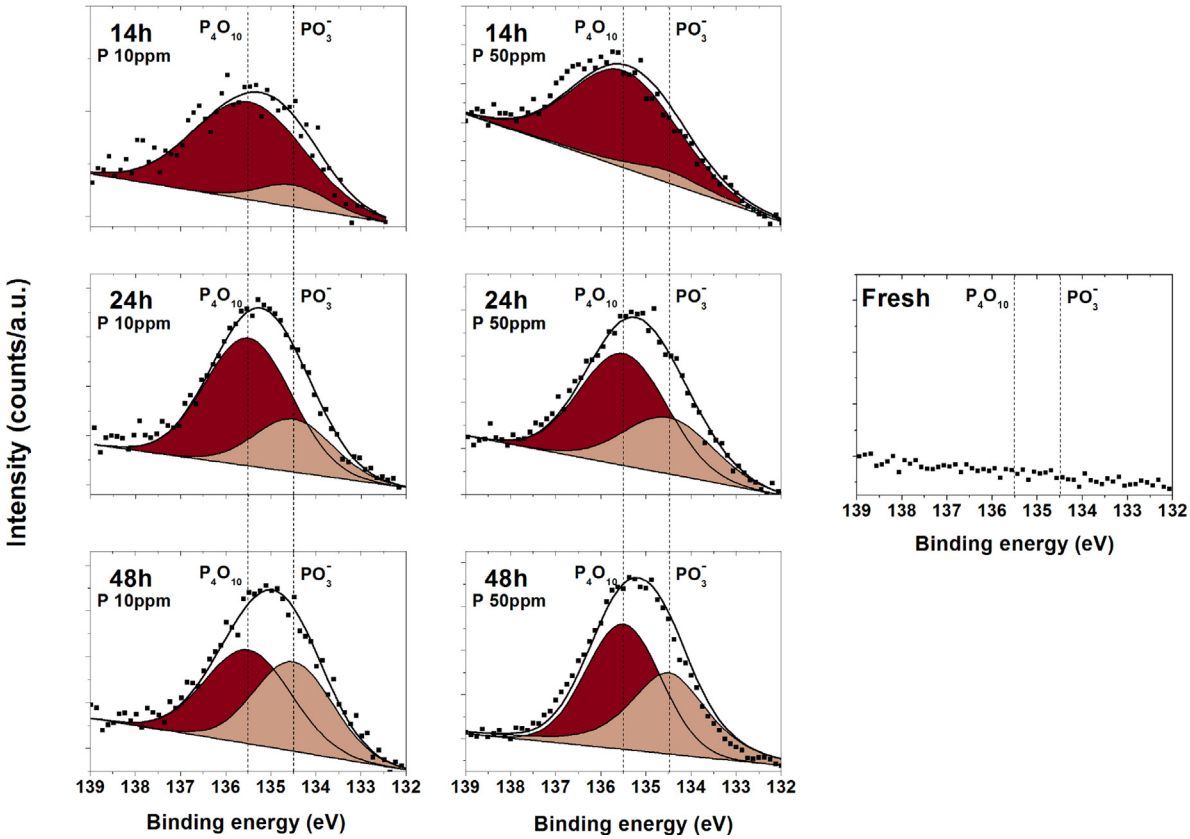

Fig. 5. Deconvolution of the P 2p XPS spectra of for all phosphorous exposed Fe-BEA catalysts compared to the fresh one. The dark and light brown peak represents P_2O_5 and PO_3^-, respectively. The sum of the deconvoluted peaks is shown by the solid black line and compared to the experimental data shown as dots.

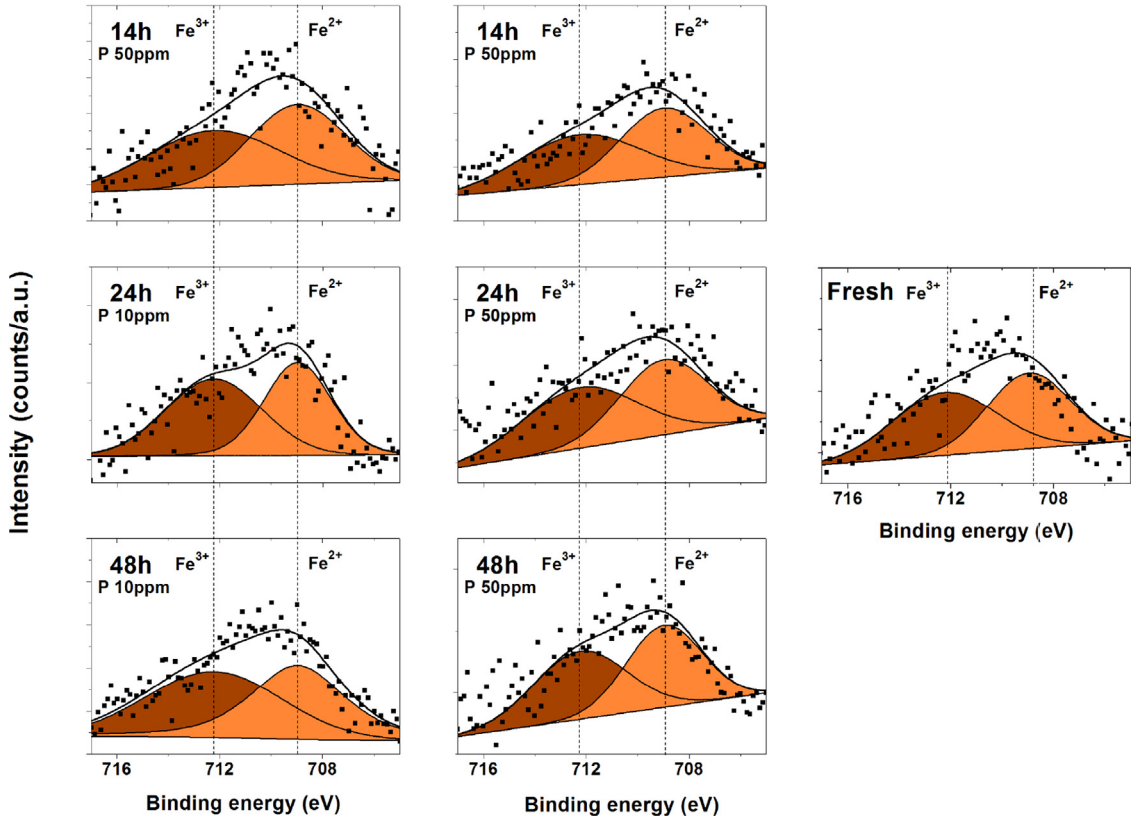

Fig. 6. Deconvolution of the Fe $2p_{3/2}$ XPS spectra of for all phosphorous exposed Fe-BEA catalysts compared to the fresh one. The dark and light orange peak represents Fe^{3+} and Fe^{2+}, respectively. The sum of the deconvoluted peaks are shown by the solid black line and compared to the experimental data shown as dots.

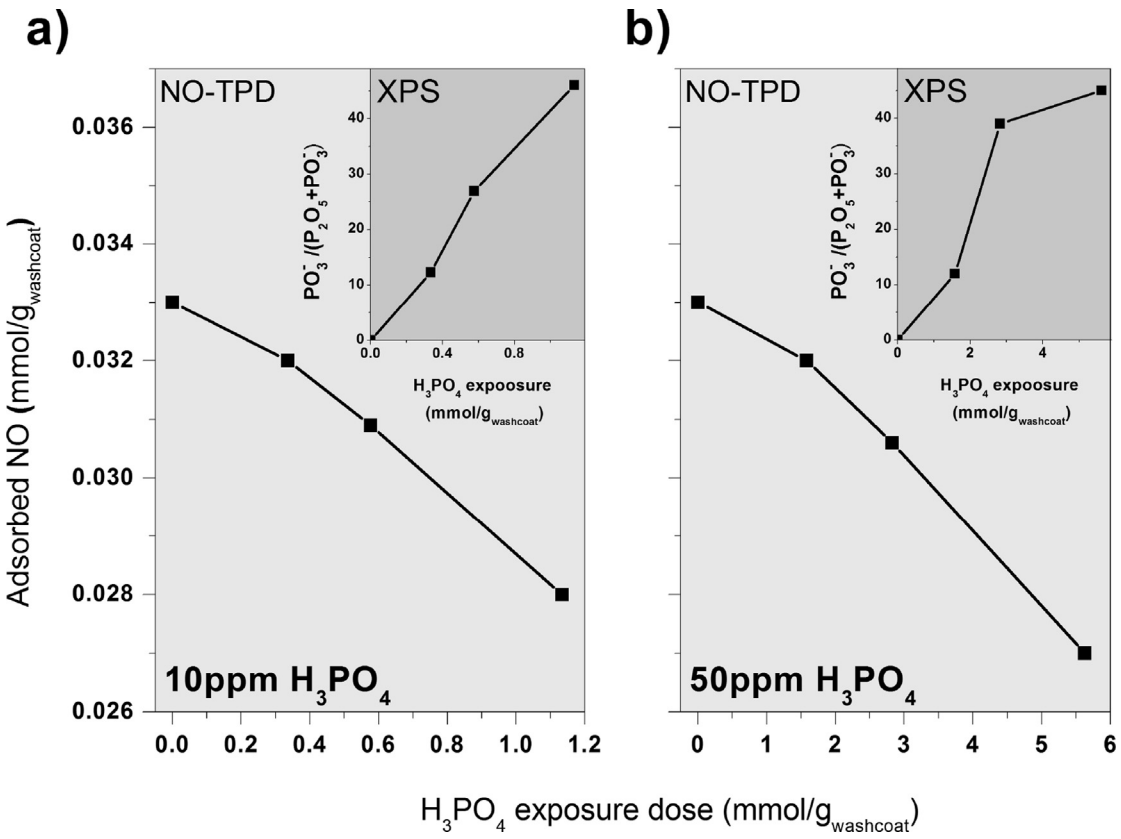

Fig. 7. Total amount of adsorbed NO during NO-TPD experiments compared to the relative concentration of PO_3^- calculated from the deconvoluted P 2p XPS spectra. The amounts are shown versus the H_3PO_4 exposure dose: (a) Fe-BEA catalysts exposed to 10 ppm H_3PO_4 for 14, 24 and 48 h; (b) Fe-BEA catalysts exposed to 50 ppm H_3PO_4 for 14, 24 and 48 h.

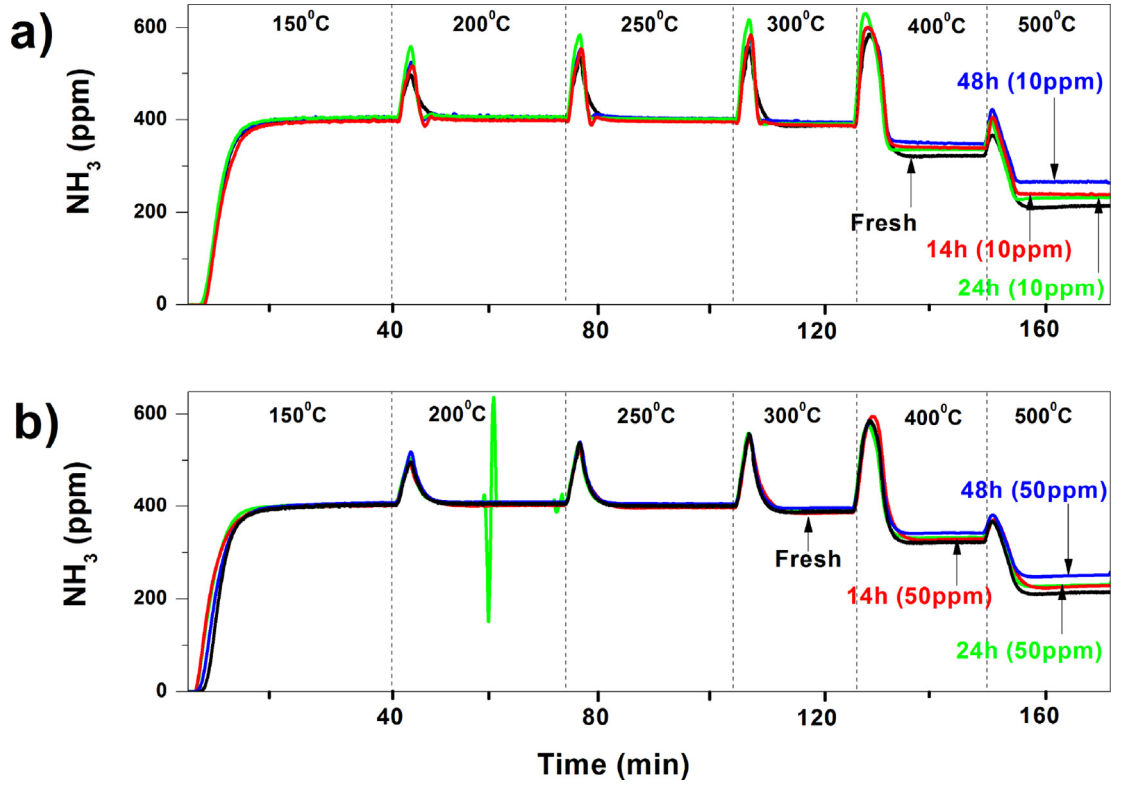

Fig. 8. Outlet NH_3 concentration during NH_3 oxidation experiments: (a) Fe-BEA atalysts exposed to 10 ppm H_3PO_4 for 14, 24 and 48 h; (b) Fe-BEA catalysts exposed to 50 ppm H_3PO_4 for 14, 24 and 48 h. The samples were exposed to 400 ppm NH_3, 8% O_2 and 5% H_2O and the temperature was stepwise increased from 150 to 500 °C (150, 200, 250, 300, 400 and 500 °C). The total flow rate was 3500 ml/min.

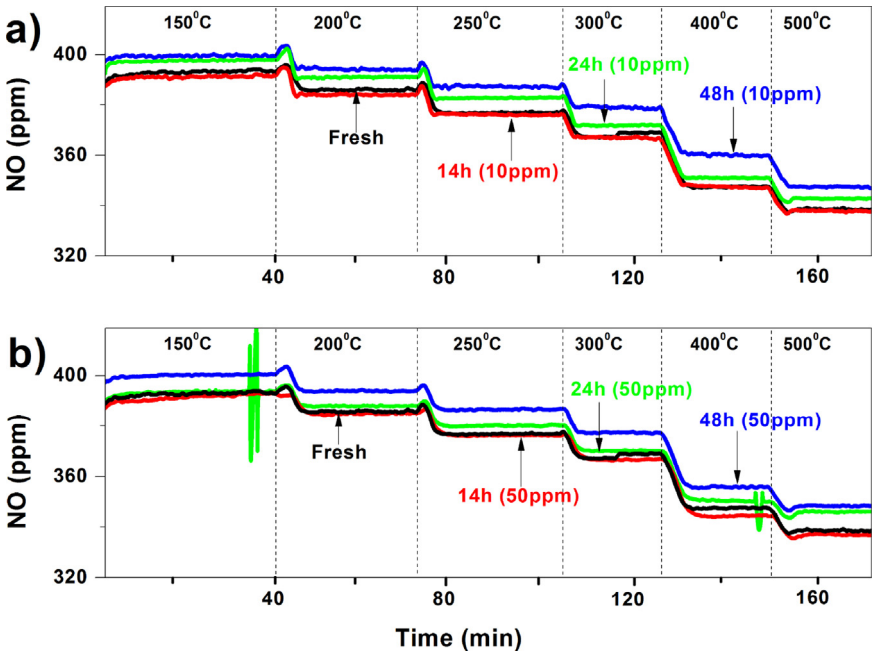

Fig. 9. Outlet NO concentration during NO oxidation experiments: (a) Fe-BEA catalysts exposed to 10 ppm H_3PO_4 for 14, 24 and 48 h; (b) Fe-BEA catalysts exposed to 50 ppm H_3PO_4 for 14, 24 and 48 h. The samples were exposed to 400 ppm NO, 8% O_2 and 5% H_2O and the temperature was stepwise increased from 150 to 500 °C (150, 200, 250, 300, 400 and 500 °C). The total flow rate was 3500 ml/min.

reaction is very slow with almost no NO_X reduction, compared to 200 °C where significant conversion of NO_X can be observed. At 250 and 300 °C the SCR reaction is markedly affected by the phosphorous exposure. However, at 400 and 500 °C the conversion of NO_X is high for all samples and no significant difference between the samples can be seen. Furthermore, when the temperature is increased from 300 to 400 °C it can be seen in Fig. 10a that the conversion of NO_X temporarily increases before reaching steady state, as well when increasing the temperature to 500 °C, the same behaviour can be observed. Fig. 10b shows the outlet concentration of NH_3. Also here ammonia is stored during the initial part of the experiment, similar to the NH_3-TPD and NH_3-oxidation experiments (cf. NH_3-TPD and NH_3-oxidation). At 150 °C the conversion of ammonia is very low, as the conversion of NO_X at same temperature. The conversion of ammonia is notable already at 200 °C and very high above 250 °C. For all samples the conversion of NH_3 is higher than the NO_X conversion which is in line with the previously observed overconsumption of ammonia during NH_3-SCR over Fe-zeolites [32,33,47,48]. Significant ammonia desorption peaks can be seen between all temperature steps except for the highest temperatures, 400 and 500 °C.

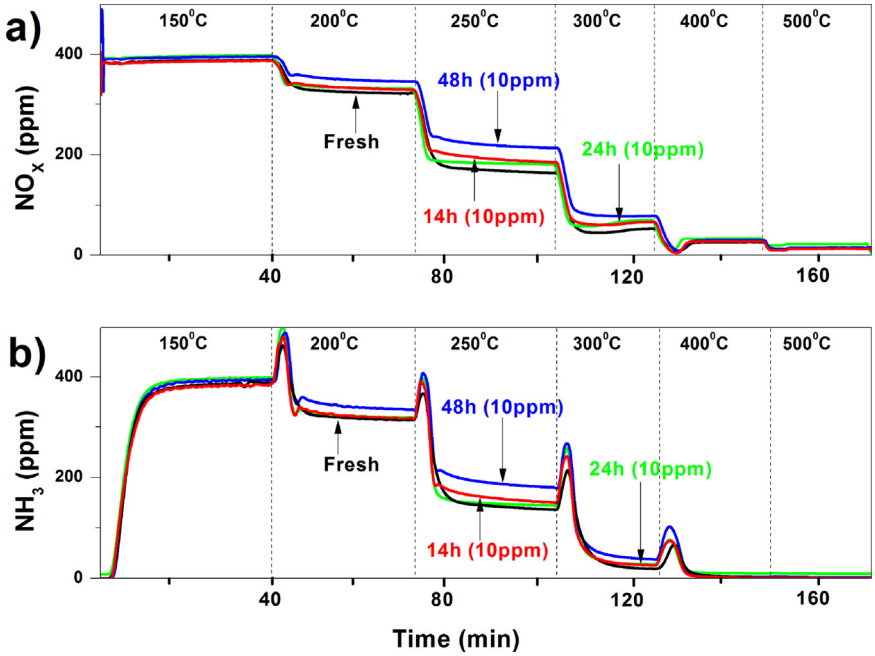

Fig. 10. Outlet of NO_X (a) and NH_3 (b) concentrations during NH_3-SCR for Fe-BEA samples exposed to 10 ppm H_3PO_4. The samples were exposed to 400 ppm NO, 400 ppm NH_3, 8% O_2 and 5% H_2O and the temperature was stepwise increased from 150 to 500 °C (150, 200, 250, 300, 400 and 500 °C). The total flow rate was 3500 ml/min.

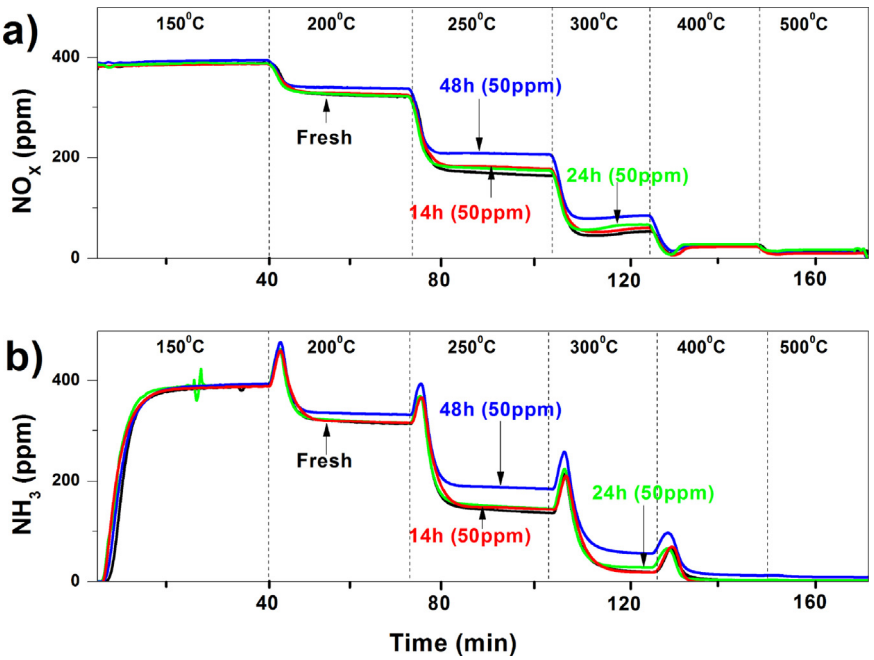

Fig. 11. Outlet of NO_X (a) and NH_3 (b) concentrations during NH_3-SCR for Fe-BEA samples exposed to 50 ppm H_3PO_4. The samples were exposed to 400 ppm NO, 400 ppm NH_3, 8% O_2 and 5% H_2O and the temperature was stepwise increased from 150 to 500 °C (150, 200, 250, 300, 400 and 500 °C). The total flow rate was 3500 ml/min.

Fig. 11a and b shows the outlet concentration of NO_X and NH_3, respectively, for the samples exposed to 50 ppm H_3PO_4 compared to the fresh sample. As for the samples exposed to 10 ppm H_3PO_4 the SCR reaction at 150 °C is very slow. However, above 150 °C there is a notable difference in NO_X conversion between the fresh and phosphorous exposed samples. The SCR activity is most affected for the sample most extensively exposed to H_3PO_4. At 400 °C the NO_X conversion is very high and at 500 °C complete NO_X conversion is reached for all samples. As for the samples exposed to 10 ppm H_3PO_4 the conversion is temporarily higher during the temperature increase at the higher temperatures until steady state is reached. Fig. 11b shows the outlet concentration of NH_3. Also for these samples ammonia storage is observed during the low-temperature step at 150 °C where the conversion of ammonia is very low, as the conversion of NO_X. The conversion of ammonia becomes higher at 200 °C and a clear difference in conversion is observed between the fresh sample and the sample most extensively exposed to H_3PO_4. At 400 and 500 °C complete NH_3 conversion is observed for the fresh sample as for the phosphorous exposed samples. Strong ammonia desorption peaks can be seen between all temperature steps except between 400 and 500 °C. An overconsumption of ammonia is also observed for the samples exposed to 50 ppm H_3PO_4.

In general, it can be observed that the deactivation due to phosphorous exposure is similar for both levels (i.e. 10 and 50 ppm H_3PO_4), as all other results have shown. However, the exposure time towards phosphoric acid is more important than the H_3PO_4 concentration during the exposure and hence a clear deactivation of the catalytic performance is observed with increasing H_3PO_4 exposure time.

3.4. Ammonia inhibition

The results for the ammonia inhibition experiments, where the samples were exposed to 400 ppm NO, 400 ppm NH_3, 8% O_2 and 5% H_2O at 200 and 250 °C, are summarized in Table 1 and displayed in Fig. 12. The samples were initially exposed to the gas mixture for 40 min and the NH_3 feed was then cut off and compensated with inert gas to maintain constant flow. The inhibition effect of ammonia for the fresh and phosphorous exposed samples can clearly be seen at the two temperatures studied. After the ammonia cut-off during the NH_3-SCR experiment at 200 °C, there is an immediate increase in NO_X reduction for about 13 min for the fresh Fe-BEA sample as well as for the samples exposed to H_3PO_4 for shortest time, 14 h (for both 10 and 50 ppm H_3PO_4). The samples exposed to 10 ppm H_3PO_4 for 24 and 48 h show an increase in NO_X reduction for about 11 and 15 min, respectively. Furthermore, the samples exposed to 50 ppm H_3PO_4 for 24 and 48 h show an increase in NO_X reduction for about 12 and 14 min, respectively. At 250 °C, the results are similar. The fresh sample and the sample with shortest exposure time for H_3PO_4 show an immediate increase in NO_X reduction for about 4 min. The samples exposed to 10 ppm H_3PO_4 for 24 and 48 h show an increase in NO_X reduction for about 3 and 5 min, respectively. Finally, the samples exposed to 50 ppm H_3PO_4 at 24 and 48 h show an increase in NO_X reduction for about 3 and 4 min, respectively. Furthermore, NO_2 production can be observed for all samples when the stored ammonia is consumed.

4. Discussion

4.1. Ammonia storage

From the ammonia TPD experiments, the effect of phosphorous exposure on the ammonia storage can clearly be seen during the temperature ramp. The ammonia storage is more affected by the exposure time rather than the concentration of phosphoric acid used. For the samples exposed with H_3PO_4 for 24 h, the desorption maximum shifts significantly towards lower temperature indicating decreased ammonia adsorption strength. However, the amount of desorbed NH_3 during the temperature ramp increases which indicates an increased amount of strongly bound ammonia compared to the fresh sample. The capacity to store ammonia is mainly related to the Brønsted acidity of the zeolite and likely also to the number of iron sites [1,34,35,49,50]. This relationship is clearly seen when comparing the decreased storage capacity of ammonia and the dealumination of metal-exchanged zeolites due to hydrothermal treatment [31–34]. Castellino et al. [24] observed

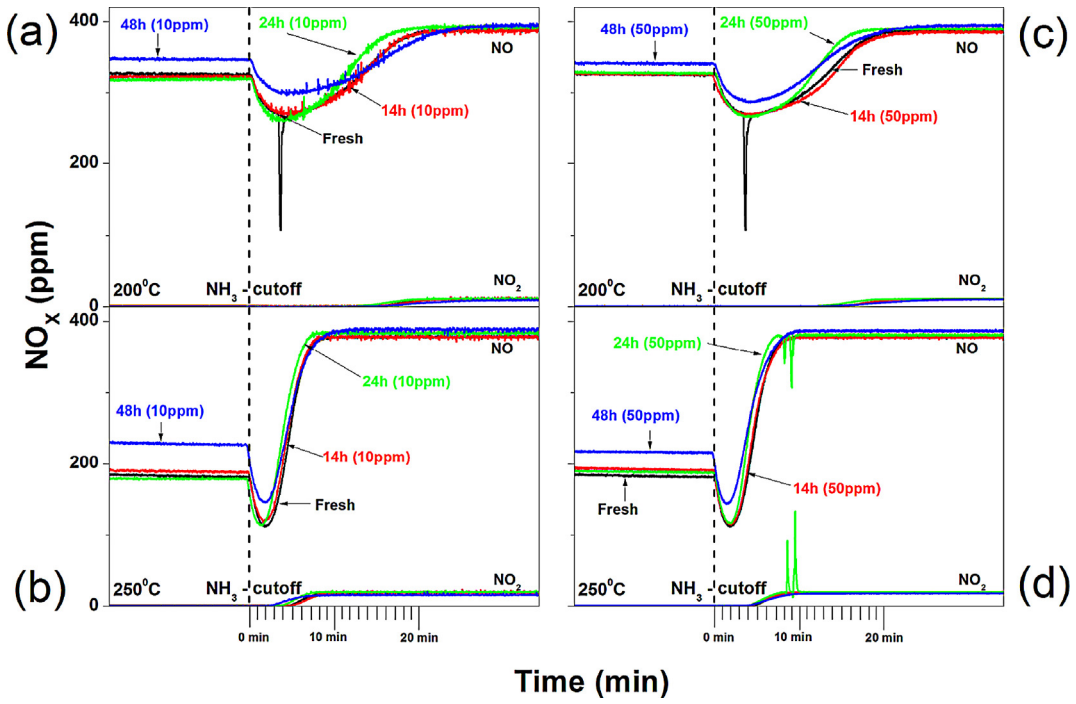

Fig. 12. Ammonia inhibition experiments for Fe-BEA samples exposed to 10 ppm H_3PO_4 for 14, 24 and 48 h at 200 °C (a) and 250 °C (b). Corresponding experiments for Fe-BEA samples exposed to 50 ppm H_3PO_4 for 14, 24 and 48 h at 200 °C (c) and 250 °C (d).

similar results for vanadia-based NH_3-SCR catalysts exposed to phosphorous, indicating an increased acidity of the catalyst with increased exposure time for phosphorous. However, in the present study we instead notice a decrease in the amount of desorbed NH_3 with further phosphorous exposure (48 h) as shown in Fig. 2. Furthermore, the NH_3 desorption maximum shifts back to higher temperatures, indicating a reverse effect with longer compared to shorter time of phosphorous exposure. This is in agreement with the studies of Kern et al. [25] and Silver et al. [23] who showed a decreased ammonia storage capacity for Fe-zeolites due to phosphorous poisoning which increased with increased exposure time for H_3PO_4. The temporarily increase in storage capacity of strongly bound ammonia in the present study may be related to the relatively high amount of phosphorous pentoxides (P_2O_5) compared to metaphosphates PO_3^- for the samples with shortest exposure time for H_3PO_4 as indicated by the XPS measurements. Longer exposure time to phosphoric acid results in a decreased relative amount of phosphorous pentoxides which seems to be correlated with the decreased amount of desorbed ammonia. Furthermore, as shown in Fig. 3, the total amount of desorbed ammonia is almost constant whereas the fraction of strongly bound ammonia increases with increased phosphorous exposure. On the contrary the amount of weakly bound ammonia follows the reverse trend with increased phosphorous exposure time and as a result the total amount of stored ammonia is almost constant. The NH_3-TPD results indicate that the number of acid sites to store stronger bound ammonia increases at the expense of sites for weakly bound ammonia likely due to formation of phosphorous pentoxides.

4.2. NO adsorption

The XPS results, summarized in Table 1 and shown in Figs. 4 and 5, clearly show that phosphorous pentoxides (P_2O_5) primarily are formed after shorter time of exposure of phosphoric acid. Furthermore, the deconvolution of the XPS spectra for phosphorous in Fig. 5 shows that metaphosphates, PO_3^-, are formed after longer time of exposure which clearly can be correlated to the results from the activity experiments. Furthermore, the deconvolution of the Fe $2p_{3/2}$ peak in Fig. 6 shows that compared to the fresh sample the oxidation state of iron is almost constant for the samples exposed to H_3PO_4. The Fe^{3+} peak in Fig. 6 represents monomeric iron (Fe^{3+}), iron particles (Fe_2O_3) and likely also trivalent oligomeric iron (Fe_XO_Y) species. The UV–vis spectrum in Fig. 1 shows that the amount of iron particles compared to monomeric iron (Fe^{3+}), which is the dominating iron species is relatively low, hence the deconvoluted Fe^{3+} peak from the XPS results mainly represents monomeric iron. However, the Fe^{2+} peak in Fig. 6 represents both divalent dimeric iron species and, to a minor extent, also divalent oligomeric iron (Fe_XO_Y) species. In a previous study by our group of the same catalyst using DRIFT-spectroscopy, it was shown that the relative amount of oligomeric iron species is high [38]. Peak III and IV in the UV–vis spectrum indicate that both dimeric and oligomeric iron species are present in the Fe-BEA sample. When correlated to the previous DRIFTS results, peak IV most likely represents oligomeric iron species hence the Fe^{2+} XPS peak originates from both types with oligomeric iron species as the dominating one. Furthermore, the NO storage experiments show a decreased storage capacity of nitric oxide with longer time of phosphorous exposure. For Fe-zeolites it has previously been shown that the NH_3-SCR activity is related to the amount of adsorbed NO [31,33,38] with monomeric (Fe—O—OH) and dimeric (OH—Fe—O—Fe—OH) iron species as the active iron sites [51]. The XPS results do not indicate any changes of the oxidation state of iron due to phosphorous exposure. However, the activity and XPS results clearly show a decreased activity with increased relative amount of metaphosphates, PO_3^-. This indicates that the decreased activity after longer time of exposure to phosphoric acid is due to adsorption of metaphosphate which replaces hydroxyl (OH^-) groups on the active iron species. Furthermore, it cannot be ruled out that phosphorous pentoxides, to a minor extent, also cause deactivation by physically blocking iron species. However, as mentioned previously, there is no significant difference in accumulation of phosphorous between the two levels of phosphorous (i.e. 10 and 50 ppm H_3PO_4) used during the exposure indicating that the formation of metaphosphates proceeds via

surface reaction and that the reaction is not restricted by the supply of H_3PO_4.

4.3. NH_3- and NO- oxidation

It has previously been shown that dimeric iron is the main active iron species for NH_3-oxidation over Fe-zeolites [51]. Furthermore, in a previous work by our group [33], it was shown that the activity for NH_3-oxidation over Fe-BEA is very sensitive to loss of active dimeric iron species. The results in the present study show a clear decrease in activity for NH_3 oxidation at high temperatures (500 °C), indicating loss of active dimeric iron sites. As previously discussed, the metaphosphates might cause deactivation of the active iron species by replacement of hydroxyl groups with metaphosphate groups. The samples exposed to phosphoric acid for 48 h are the most severely deactivated catalysts. The results from the deconvolution of the XPS spectra, summarized in Table 1, show that about 50% of the accumulated phosphorous in the samples is present as metaphosphates, PO_3^-, which most likely have blocked the access to some of the active sites on dimeric iron species when correlated to the NH_3-oxidation activity. Furthermore, the activity for NO-oxidation is less affected by phosphorous. Devadas et al. [52], have recently showed that NO oxidation occurs over Fe_2O_3 particles in iron-exchanged zeolites. The results from the NO oxidation experiments in the present study show a stepwise decrease in activity with increased phosphorous accumulation. This indicates that the active iron particles most likely become physically blocked by phosphorous pentoxides. However, it should not be ruled out that adsorbed phosphorous also chemically might affect the catalytic properties of the active iron particles.

4.4. Selective catalytic reduction of NO_X with NH_3

The NH_3-SCR experiments show similar results for the different levels of phosphorous exposure (i.e. 10 and 50 ppm H_3PO_4). As previously mentioned, Brandenberger et al. [51] have shown that monomeric (Fe—O—OH) and dimeric (OH—Fe—O—Fe—OH) iron species are the active iron sites for low- and high-temperature SCR, respectively. The results in the present study show that the low-temperature NH_3-SCR reaction is affected by the phosphorous exposure while the corresponding high-temperature reaction is not significantly affected by the phosphorous exposure. However, the NH_3-oxidation experiment (c.f. NH_3-oxidation) shows a decrease in activity indicating a decrease of the number of active dimeric sites. Furthermore, Devas et al. [52] showed that NO oxidation over Fe_2O_3 particles in the zeolite is the rate determining step for the NH_3-SCR reaction over Fe-ZSM-5. The decrease in NO-oxidation at high temperatures and the deactivation of dimeric iron sites do not seem to affect the NO_X conversion negatively during high-temperature NH_3-SCR. As previously shown for the same type of catalyst [32,33], a large fraction of the active sites in the catalyst is not used at high temperatures (> 400 °C) due to high reaction rates. To observe a significant decrease in NO_X reduction at high temperatures, a strong deactivation with a considerable loss of active iron sites must proceed. However, at lower temperatures (250 and 300 °C) the NH_3-SCR reaction shows a significant decrease in activity, indicating a decrease in number of available active sites after longer time of phosphorous exposure. This is well in accordance with the XPS results, showing that the amount of accumulated metaphosphates, PO_3^- increases after longer time of phosphorous exposure, indicating that the metaphosphates interact and chemically block the monomeric iron species active for NO_X reduction by replacing hydroxyl with metaphosphate groups.

Furthermore, phosphorous exposure of Fe-BEA in the present study shows a lower deactivation of the NO_X reduction performance when compared to our previous studies of hydrothermally treated Fe-BEA between 600 and 700 °C for 3–100 h [31–33,38,39]. However, due to the continuous exposure of phosphorous in commercial exhaust aftertreatment systems, the chemical deactivation due to phosphorous may be more significant after long time exposure.

4.5. Ammonia inhibition

The ammonia inhibition experiments show a clear trend when correlated to the ammonia storage capacity. The effect of high coverage of ammonia, inhibiting the NH_3-SCR reaction is well known from previous studies [1,10,35,53]. After the NH_3 cut-off, ammonia spills over from the acidic sites to the active iron species and reacts with adsorbed NO_X until all available ammonia is consumed. The period with increased NO_X reduction after the ammonia cut-off, decreases with increased phosphorous exposure (for 14 and 24 h). The ammonia storage experiments show a significant increase in ammonia storage capacity after short time of phosphorous exposure. However, the period with increased NO_X reduction after the ammonia cut-off decreases with increasing phosphorous exposure (i.e. 24 h of H_3PO_4 exposure with highest ammonia storage capacity). This indicates that the increased amount of strongly bound ammonia due to phosphorous exposure does not participate in buffering the active iron sites with ammonia during the NH_3-SCR reaction. This effect will result in a lower SCR performance during transient conditions. Furthermore, for the most extensively phosphorous exposed samples (48 h), a similar period with increased NO_X reduction is observed as for the fresh sample. However, the phosphorous exposed sample (48 h) has a significantly lower activity during steady-state, hence more ammonia is available for the NH_3-SCR reaction and thus the period with increased NO_X reduction is longer compared to the less H_3PO_4 exposed samples.

5. Concluding remarks

The aim of the present study is to gain fundamental understanding of the chemical deactivation mechanisms of Fe-BEA as NH_3-SCR catalyst using phosphoric acid as the catalyst poison. The focus is paid on the interaction between the active iron species and phosphorous by correlating the catalytic performance with the results of different catalyst characterization techniques.

The Fe-BEA samples were exposed to 10 and 50 ppm phosphoric acid for 14, 24 and 48 h. The results show that the degree of deactivation is strongly dependent of the phosphorous exposure time. However, the rate of deactivation is the same for 10 and 50 ppm H_3PO_4.

The deconvoluted P 2p XPS peak shows that phosphorous pentoxides (P_2O_5) primarily are formed after short time of exposure to phosphoric acid while longer time of exposure results in formation of metaphosphates (PO_3^-). The relative amount of metaphosphates compared to phosphorous pentoxides is about 45% after 48 h of phosphorous exposure (for both 10 and 50 ppm H_3PO_4). Furthermore, the deconvolution of the Fe $2p_{3/2}$ peak does not show any significant change in oxidation state of iron after phosphorous exposure. However, the NO-TPD experiments show a decreased number of adsorption sites for nitric oxide with a relative increase of metaphosphates.

The decreased activity during NH_3-oxidation due to phosphorous exposure indicates a decreased number of dimeric iron sites (OH—Fe—O—Fe—OH), which are the active iron species for NH_3-oxidation. There is a significant decrease in the oxidation rate of ammonia for the samples most severely exposed to phosphorous (48 h). This indicates that the deactivation may be due to the relative increase of metaphosphates, which replace hydroxyl groups on the active iron sites. Furthermore, the activity for NO oxidation,

decreases slowly for all samples exposed to phosphorous, indicating that the phosphorous pentoxides on the surface may block the active iron particles which are the active sites for NO-oxidation.

The decreased activity during NH_3-SCR at low temperatures (150–300 °C) indicates a substantial decrease of available monomeric iron sites (Fe—O—OH), which is the crucial site for low-temperature SCR. The results indicate that the relative increase of metaphosphates, with increasing phosphorous exposure results in replacement of hydroxyl groups with metaphosphate groups on the monomeric iron sites as well. Furthermore, there is no significant activity decrease during high-temperature SCR (400–500 °C), even though the NH_3-oxidation indicates a decreased number of accessible sites on dimeric iron species, which provides the sites for the rate-limiting reaction step at high-temperature SCR. However, at higher temperatures a large fraction of the catalyst is not used due to high reaction rates and the deactivation must be very severe until it can be observed.

The NH_3-inibiting experiments show a decreased period with improved NO_X conversion due to phosphorous deactivation, although the NH_3-TPD experiments show an increased storage capacity of strongly bound ammonia. These results show that the increased amount of strongly bound ammonia due to phosphorous exposure does not participate in buffering the active iron sites with ammonia during NH_3-SCR.

Exposure of Fe-BEA to phosphoric acid results in chemical deactivation of the catalyst. We propose that the deactivation proceeds in two steps; (i) shorter time of phosphorous exposure results in formation of phosphorous pentoxides, P_2O_5, with a relatively low amount of metaphosphates, PO_3^-, which do not affect the NO_X conversion but results in increased amount of strongly bound ammonia not active in the SCR reaction, and (ii) longer time of phosphorous exposure results in continued increase of the relative amount of metaphosphates which results in significantly decreased NO_X conversion, especially during low-temperature NH_3-SCR, by replacing the hydroxyl groups on the active iron species.

Acknowledgments

This work has been performed within the FFI program (Proj. No. 32900-1), which is financially supported by the Swedish Energy Agency and partly within the Competence Centre for Catalysis, which is hosted by Chalmers University of Technology and financially supported by the Swedish Energy Agency and the member companies AB Volvo, ECAPS AB, Haldor Topsøe A/S, Scania CV AB and Volvo Car Corporation AB. Financial support from Knut and Alice Wallenberg Foundation, Dnr KAW 2005.0055, is gratefully acknowledged. The authors would also like to thank Volvo Group Trucks Technology and Miroslawa Milh for help with the chemical deactivation of the samples.

References

[1] S. Brandenberger, O. Krocher, A. Tissler, R. Althoff, Catalysis Reviews – Science and Engineering 50 (2008) 492–531.
[2] H. Sjövall, L. Olsson, E. Fridell, R.J. Blint, Applied Catalysis B: Environmental 64 (2006) 180–188.
[3] K. Rahkamaa-Tolonen, T. Maunula, M. Lomma, M. Huuhtanen, R.L. Keiski, Catalysis Today 100 (2005) 217–222.
[4] S. Kieger, G. Delahay, B. Coq, B. Neveu, Journal of Catalysis 183 (1999) 267–280.
[5] J.H. Park, H.J. Park, J.H. Baik, I.S. Nam, C.H. Shin, J.H. Lee, B.K. Cho, S.H. Oh, Journal of Catalysis 240 (2006) 47–57.
[6] J.A. Sullivan, J. Cunningham, M.A. Morris, K. Keneavey, Applied Catalysis B: Environmental 7 (1995) 137–151.
[7] H. Sjövall, E. Fridell, R. Blint, L. Olsson, Topics in Catalysis 42–43 (2007) 113–117.
[8] A. Grossale, I. Nova, E. Tronconi, D. Chatterjee, M. Weibel, Journal of Catalysis 256 (2008) 312–322.
[9] A. Grossale, I. Nova, E. Tronconi, Catalysis Today 136 (2008) 18–27.
[10] O. Kröcher, M. Devadas, M. Elsener, A. Wokaun, N. Söger, M. Pfeifer, Y. Demel, L. Mussmann, Applied Catalysis B: Environmental 66 (2006) 208–216.
[11] A. Grossale, I. Nova, E. Tronconi, Catalysis Letters 130 (2009) 525–531.
[12] P. Forzatti, L. Lietti, I. Nova, E. Tronconi, Catalysis Today 151 (2010) 202–211.
[13] K. Kamasamudram, N.W. Currier, X. Chen, A. Yezerets, Catalysis Today 151 (2010) 212–222.
[14] K. Kamasamudram, N.W. Currier, T. Szailer, A. Yezerets, SAE International Journal of Fuels and Lubricants 3 (2010) 664–672.
[15] S. Brandenberger, O. Krocher, A. Tissler, R. Althoff, Industrial & Engineering Chemistry Research 50 (2011) 4308–4319.
[16] C.H. Bartholomew, Applied Catalysis A: General 212 (2001) 17–60.
[17] V. Kröger, Poisoning of Automotive Exhaust Gas Catalyst Components, Process and Environmental Engineering, University of Oulu, Oulu, Finland, 2007.
[18] L. Ma, J.H. Li, Y.S. Cheng, C.K. Lambert, L.X. Fu, Environmental Science & Technology 46 (2012) 1747–1754.
[19] J. Li, R. Zhu, Y. Cheng, C.K. Lambert, R.T. Yang, Environmental Science & Technology 44 (2010) 1799–1805.
[20] C. He, Y. Wang, Y. Cheng, C.K. Lambert, R.T. Yang, Applied Catalysis A: General 368 (2009) 121–126.
[21] T.R.C. Zezza, M.d.S. Castilho, N.R. Stradiotto, Fuel 95 (2012) 15–18.
[22] O. Kröcher, M. Elsener, Applied Catalysis B: Environmental 77 (2008) 215–227.
[23] R.G. Silver, M.O. Stefanick, B.I. Todd, Catalysis Today 136 (2008) 28–33.
[24] F. Castellino, S.B. Rasmussen, A.D. Jensen, J.E. Johnsson, R. Fehrmann, Applied Catalysis B: Environmental 83 (2008) 110–122.
[25] P. Kern, M. Klimczak, T. Heinzelmann, M. Lucas, P. Claus, Applied Catalysis B: Environmental 95 (2010) 48–56.
[26] D. Nicosia, I. Czekaj, O. Kröcher, Applied Catalysis B: Environmental 77 (2008) 228–236.
[27] F. Castellino, A.D. Jensen, J.E. Johnsson, R. Fehrmann, Applied Catalysis B: Environmental 86 (2009) 196–205.
[28] F. Castellino, A.D. Jensen, J.E. Johnsson, R. Fehrmann, Applied Catalysis B: Environmental 86 (2009) 206–215.
[29] J. Blanco, P. Avila, C. Barthelemy, A. Bahamonde, J.A. Odriozola, J.F.G. De La Banda, H. Heinemann, Applied Catalysis 55 (1989) 151–164.
[30] J. Beck, J. Brandenstein, S. Unterberger, K.R.G. Hein, Applied Catalysis B: Environmental 49 (2004) 15–25.
[31] S. Shwan, R. Nedyalkova, J. Jansson, J. Korsgren, L. Olsson, M. Skoglundh, Topics in Catalysis (2013) 1–9.
[32] S. Shwan, R. Nedyalkova, J. Jansson, J. Korsgren, L. Olsson, M. Skoglundh, Industrial & Engineering Chemistry Research 51 (2012) 12762–12772.
[33] S. Shwan, J. Jansson, J. Korsgren, L. Olsson, M. Skoglundh, Catalysis Today 197 (2012) 24–37.
[34] S. Brandenberger, O. Kröcher, M. Casapu, A. Tissler, R. Althoff, Applied Catalysis B: Environmental 101 (2011) 649–659.
[35] S. Brandenberger, O. Kröcher, A. Wokaun, A. Tissler, R. Althoff, Journal of Catalysis 268 (2009) 297–306.
[36] M. Koebel, M. Elsener, Industrial & Engineering Chemistry Research 37 (1998) 327–335.
[37] M. Koebel, M. Elsener, Chemical Engineering Science 53 (1998) 657–669.
[38] S. Shwan, E. Adams, J. Jansson, M. Skoglundh, Catalysis Letters 143 (2013) 43–48.
[39] R. Nedyalkova, S. Shwan, M. Skoglundh, L. Olsson, Applied Catalysis B: Environmental 138–139 (2013) 373–380.
[40] L. Olsson, E. Fridell, Journal of Catalysis 210 (2002) 340–353.
[41] T. Yamashita, P. Hayes, Applied Surface Science 254 (2008) 2441–2449.
[42] S. Brandenberger, O. Kröcher, A. Tissler, R. Althoff, Applied Catalysis A: General 373 (2010) 168–175.
[43] M.S. Kumar, M. Schwidder, W. Grünert, A. Brückner, Journal of Catalysis 227 (2004) 384–397.
[44] M.M.J. Treacy, J.B. Higgins, Collection of Simulated XRD Powder Patterns for Zeolites, 4th ed., Elsevier, Amsterdam, The Netherlands, 2001.
[45] B. Modhera, M. Chakraborty, P.A. Parikh, R.V. Jasra, Crystal Research and Technology 44 (2009) 379–385.
[46] M. Jansen, B. Luer, Zeitschrift für Kristallographie 177 (1986) 149–151.
[47] H. Sjövall, R.J. Blint, A. Gopinath, L. Olsson, Industrial & Engineering Chemistry Research 49 (2010) 39–52.
[48] R. Nedyalkova, K. Kamasamudram, N.W. Currier, J. Li, A. Yezerets, L. Olsson, Journal of Catalysis 299 (2013) 101–108.
[49] H. Sjövall, R.J. Blint, L. Olsson, Journal of Physical Chemistry C 113 (2009) 1393–1405.
[50] I. Nova, C. Ciardelli, E. Tronconi, D. Chatterjee, B. Bandl-Konrad, AIChE Journal 52 (2006) 3222–3233.
[51] S. Brandenberger, O. Kröcher, A. Tissler, R. Althoff, Applied Catalysis B: Environmental 95 (2010) 348–357.
[52] M. Devadas, O. Kröcher, M. Elsener, A. Wokaun, G. Mitrikas, N. Söger, M. Pfeifer, Y. Demel, L. Mussmann, Catalysis Today 119 (2007) 137–144.
[53] M. Wallin, C.J. Karlsson, M. Skoglundh, A. Palmqvist, Journal of Catalysis 218 (2003) 354–364.
[54] J.E. Thomas, C.F. Jones, W.M. Skinner, R.S.C. Smart, Geochimica et Cosmochimica Acta 62 (1998) 1555–1565.
[55] J.F. Moulder, W. Stickle, P.E. Sobol, K.D. Bomben, Handbook of X-ray Photoelectron Spectroscopy, Perkin Elmer Corporation, Eden Prairie, MN, 1992.
[56] N.S. McIntyre, D.G. Zetaruk, Analytical Chemistry 49 (1977) 1521–1529.
[57] A.R. Pratt, D.W. Blowes, C.J. Ptacek, Environmental Science & Technology 31 (1997) 2492–2498.
[58] J. Janas, J. Gurgul, R.P. Socha, T. Shishido, M. Che, S. Dzwigaj, Applied Catalysis B: Environmental 91 (2009) 113–122.